Fabrication of bimetallic-doped materials derived from a Cu-based complex for enhanced dye adsorption and iodine capture

Ai-Ai Yang,[a] Jian-Peng Cui,[a] Yu Liu,[a*] Xiao-Sa Zhang,[a] Ze-Bang Sun,[a] Nan Luo,[a] Wen-Ze Li,[a*] and Jian Luan[b*]

[a] *College of Science, Shenyang University of Chemical Technology, Shenyang, 110142, P. R. China*

[b] *College of Sciences, Northeastern University, Shenyang, 110819, P. R. China*

E-mails: wzli@syuct.edu.cn (W. Z. Li); 2010044@stu.neu.edu.cn (J. Luan)

Table S1 Selected bond distances (Å) and angles (°) for complex **1**.

Cu(1)–O(3)#1	1.950(4)	O(11)–Cu(2)–O(6)	89.68(17)
Cu(1)–O(4)#2	1.957(4)	O(9)–Cu(2)–O(8)#1	88.62(16)
Cu(1)–O(2)#3	1.970(4)	O(11)–Cu(2)–O(8)#1	167.24(15)
Cu(1)–O(1)	1.976(3)	O(6)–Cu(2)–O(8)#1	90.47(17)
Cu(1)–N(1)	2.184(4)	O(9)–Cu(2)–N(2)	103.51(17)
Cu(1)–Cu(1)#3	2.5935(10)	O(11)–Cu(2)–N(2)	104.04(17)
O(1W)–Cu(3)	2.134(3)	O(6)–Cu(2)–N(2)	88.99(17)
Cu(2)–O(9)	1.964(4)	O(8)#1–Cu(2)–N(2)	88.72(17)
Cu(2)–O(11)	1.973(4)	O(9)–Cu(2)–Cu(3)	86.89(10)
Cu(2)–O(6)	1.981(4)	O(11)–Cu(2)–Cu(3)	86.35(10)
Cu(2)–O(8)#1	1.995(4)	O(6)–Cu(2)–Cu(3)	80.60(11)
Cu(2)–N(2)	2.180(4)	O(8)#1–Cu(2)–Cu(3)	81.09(10)
Cu(2)–Cu(3)	2.5933(8)	N(2)–Cu(2)–Cu(3)	165.31(14)
O(2)–Cu(1)#3	1.970(4)	C(19)–O(2)–Cu(1)#3	122.7(3)
Cu(3)–O(10)	1.932(4)	C(16)–N(2)–Cu(2)	119.8(4)
Cu(3)–O(12)	1.956(3)	C(17)–N(2)–Cu(2)	117.3(4)
Cu(3)–O(5)	1.976(4)	O(10)–Cu(3)–O(12)	92.19(15)
Cu(3)–O(7)#1	1.984(3)	O(10)–Cu(3)–O(5)	170.16(15)
O(3)–Cu(1)#4	1.950(4)	O(12)–Cu(3)–O(5)	88.20(15)
O(4)–Cu(1)#2	1.957(4)	O(10)–Cu(3)–O(7)#1	89.49(16)
O(7)–Cu(3)#4	1.984(3)	O(12)–Cu(3)–O(7)#1	169.78(14)

O(8)–Cu(2)#4	1.995(4)	O(5)–Cu(3)–O(7)#1	88.43(15)
O(3)#1–Cu(1)–O(4)#2	169.33(14)	O(10)–Cu(3)–O(1W)	95.29(14)
O(3)#1–Cu(1)–O(2)#3	89.50(16)	O(12)–Cu(3)–O(1W)	96.88(13)
O(4)#2–Cu(1)–O(2)#3	89.83(16)	O(5)–Cu(3)–O(1W)	94.42(14)
O(3)#1–Cu(1)–O(1)	89.12(17)	O(7)#1–Cu(3)–O(1W)	93.00(14)
O(4)#2–Cu(1)–O(1)	89.59(17)	O(10)–Cu(3)–Cu(2)	82.19(10)
O(2)#3–Cu(1)–O(1)	169.44(14)	O(12)–Cu(3)–Cu(2)	82.21(10)
O(3)#1–Cu(1)–N(1)	94.59(15)	O(5)–Cu(3)–Cu(2)	88.13(10)
O(4)#2–Cu(1)–N(1)	96.07(15)	O(7)#1–Cu(3)–Cu(2)	88.03(10)
O(2)#3–Cu(1)–N(1)	96.51(14)	O(1W)–Cu(3)–Cu(2)	177.27(10)
O(1)–Cu(1)–N(1)	94.04(14)	C(26)–O(3)–Cu(1)#4	122.9(3)
O(3)#1–Cu(1)–Cu(1)#3	84.79(10)	C(26)–O(4)–Cu(1)#2	123.1(3)
O(4)#2–Cu(1)–Cu(1)#3	84.55(10)	C(27)–O(5)–Cu(3)	118.3(3)
O(2)#3–Cu(1)–Cu(1)#3	84.59(10)	C(27)–O(6)–Cu(2)	127.1(3)
O(1)–Cu(1)–Cu(1)#3	84.86(10)	C(32)–O(7)–Cu(3)#4	118.8(3)
N(1)–Cu(1)–Cu(1)#3	178.74(12)	C(32)–O(8)–Cu(2)#4	127.0(3)
C(5)–N(1)–Cu(1)	124.1(3)	C(35)–O(9)–Cu(2)	119.1(3)
C(1)–N(1)–Cu(1)	118.8(3)	C(35)–O(10)–Cu(3)	126.1(3)
C(19)–O(1)–Cu(1)	122.7(3)	C(42)–O(11)–Cu(2)	119.1(3)
O(9)–Cu(2)–O(11)	88.48(17)	C(42)–O(12)–Cu(3)	125.1(3)
O(9)–Cu(2)–O(6)	167.44(15)		

Symmetry codes: #1 $x - 1, y, z$; #2 $-x + 2, -y - 1, -z + 1$; #3 $-x + 1, -y - 1, -z + 1$; #4 $x + 1, y, z$.

Table S2 Hydrogen bonding geometries (Å, °) of complex **1**.

D–H···A	D–H	H···A	D···A	D–H···A
O2W–H2WB···O11^{i}	0.85	2.37	3.1852	162
N3–H3A···O14^{ii}	0.86	2.08	2.9126	161
O3W–H3WA···O14^{ii}	0.85	1.99	2.7996	159
O3W–H3WB···O13^{iii}	0.85	1.87	2.6848	161
N4–H4B···O2W^{iii}	0.86	2.08	2.9001	159

Symmetry codes: ^{i} $x, -1 + y, z$; ^{ii} $-x, 1 - y, -z$; ^{iii} $1 - x, 1 - y, -z$.

Table S3 Adsorption capacities of different adsorbents for CR.

Materials	Material weigh (mg)	C_0 (mg g^{-1})	Adsorption capacity (mg g^{-1})	Adsorption time (min)	Ref.
CS-VTM composite	80	100	62.20	2880	S1
f-MWCNTs	20	400	148.00	150	S2
MWCNTs	5	10	67.30	10	S3
C-Mo-1	5	80	1304.00	240	S4
$Fe_xCo_{3-x}O_4$ nanoparticle	50	20	126.86	240	S5
BMC-0.05	50	100	290.48	60	S6
C-N-1	10	80	1357.00	240	This work
C-V-1	10	80	1501.00	180	This work

Table S4 Organic dyes with different charge types and sizes.

Dye	Formula	Charge type	Size (nm × nm × nm)
Methylene Blue (MB)	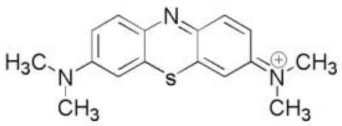	Cationic	0.40 × 0.79 × 1.63
Rhodamine B (RhB)	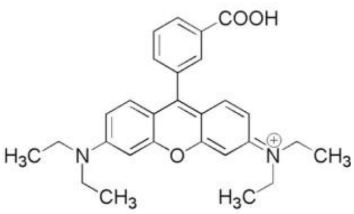	Cationic	0.68 × 1.18 × 1.57
Gentian Violet (GV)	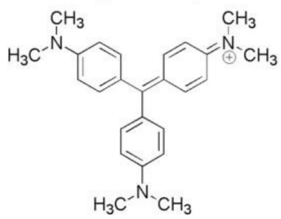	Cationic	0.40 × 1.30 × 1.37
Congo Red (CR)	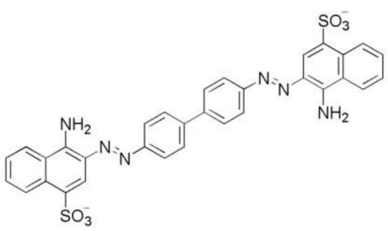	Anionic	0.39 × 0.86 × 2.61

Table S5 The parameters of pseudo-second-order, intra-particle diffusion and Elovich models in **C-N-1**.

Kinetic model	Parameters	I_2, 5 mL, 0.01 mol L^{-1}
	q_e (mg g^{-1})	0.0025
Pseudo-second-order model	k_2 (g mg^{-1} min^{-1})	8.19×10^{-4}
	R^2	0.9978
	k_{id} (mg g^{-1} $min^{-1/2}$)	277.50
Intra-particle diffusion model	C (mg g^{-1})	160.95
	R^2	0.8198
	β (g mg^{-1})	0.0013
Elovich	α (mg g^{-1} min^{-1})	254.92
	R^2	0.9716

Table S6 The parameters of pseudo-second-order, intra-particle diffusion and Elovich models in **C-V-1**.

Kinetic model	Parameters	I_2, 5 mL, 0.01 mol L^{-1}
	q_e (mg g^{-1})	0.0016
Pseudo-second-order model	k_2 (g mg^{-1} min^{-1})	8.12×10^{-4}
	R^2	0.9985
	k_{id} (mg g^{-1} $min^{-1/2}$)	367.83
Intra-particle diffusion model	C (mg g^{-1})	160.77
	R^2	0.7254
	β (g mg^{-1})	0.0011
Elovich	α (mg g^{-1} min^{-1})	333.64
	R^2	0.9552

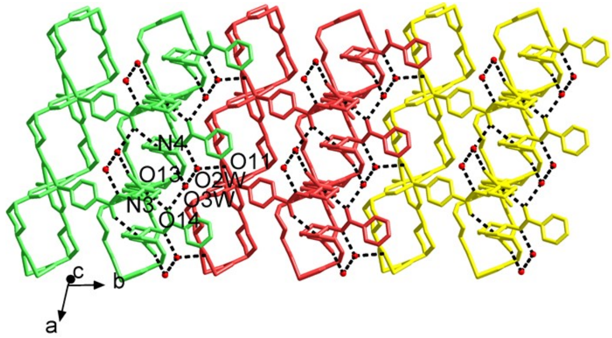

Fig. S1 The 2D supermolecule layer of complex **1**.

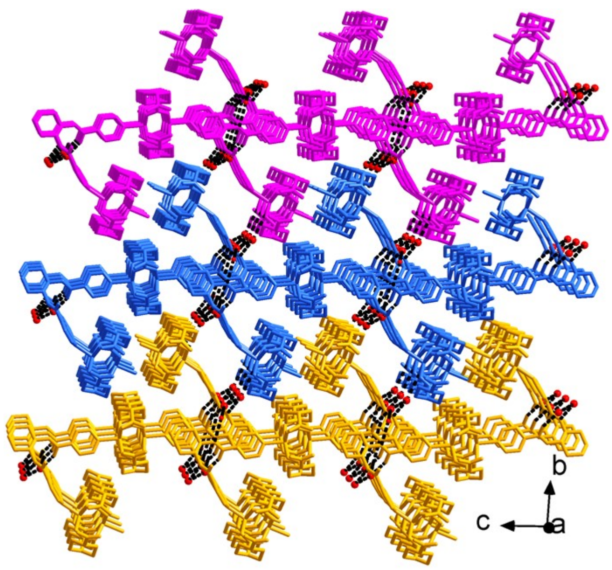

Fig. S1 The 3D supermolecule network of complex **1**.

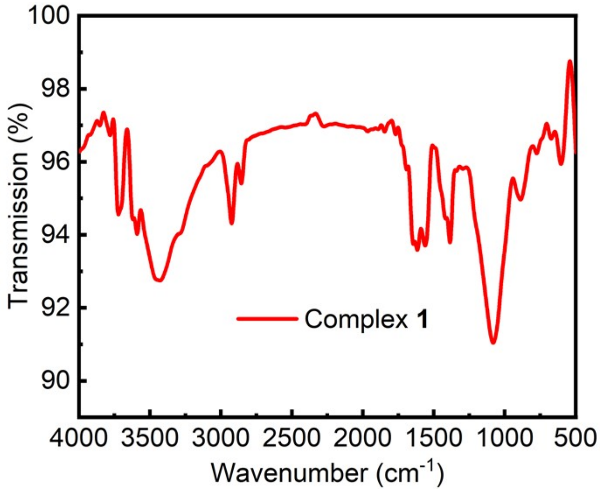

Fig. S3 The IR spectrum of complex **1**.

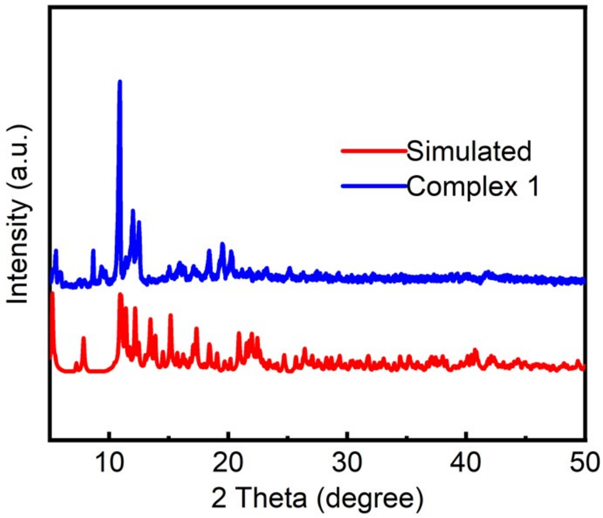

Fig. S4 The PXRD patterns of complex **1**.

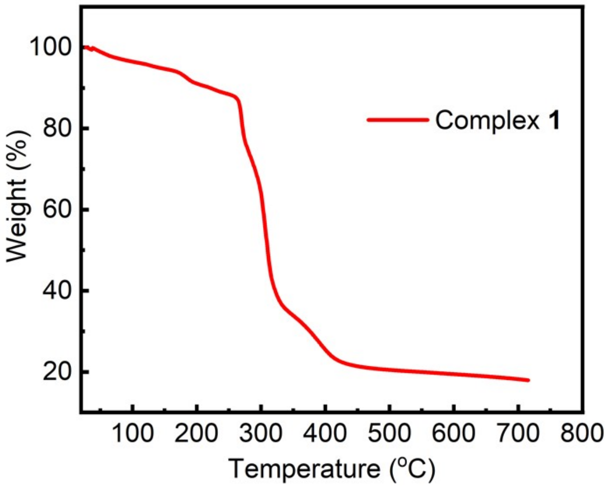

Fig. S5 The TGA curve of complex **1**.

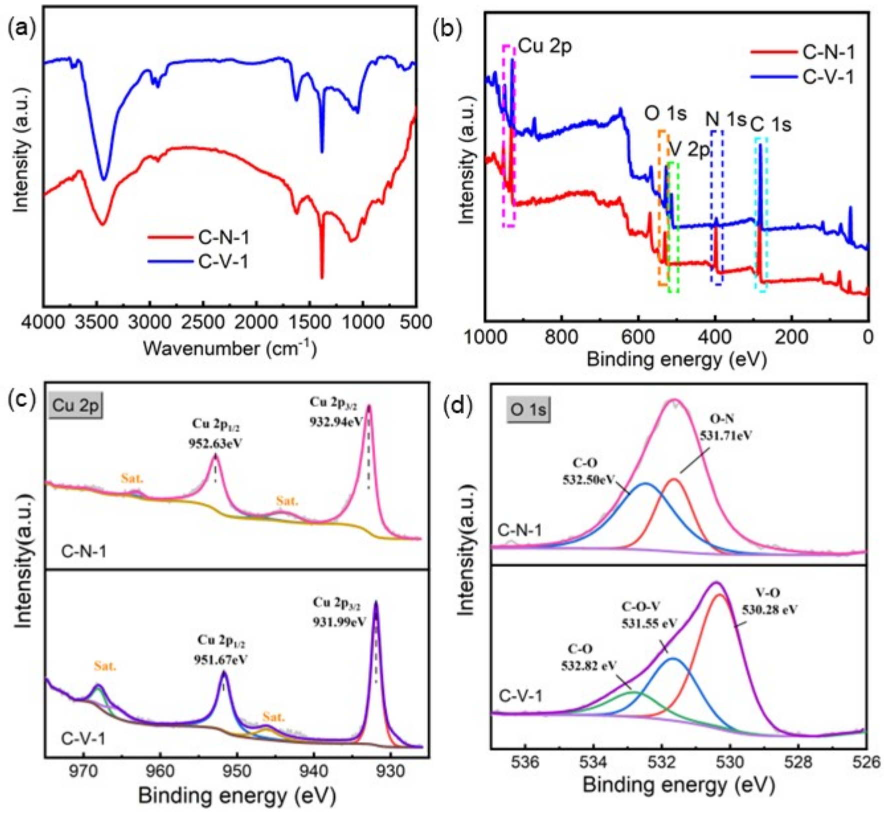

Fig. S6 (a) FT-IR spectra of **C-N-1** and **C-V-1**. (b) Survey XPS spectra of **C-N-1** and **C-V-1**. High-resolution spectra of Cu 2p (c), and O 1s (d) for **C-N-1** and **C-V-1**.

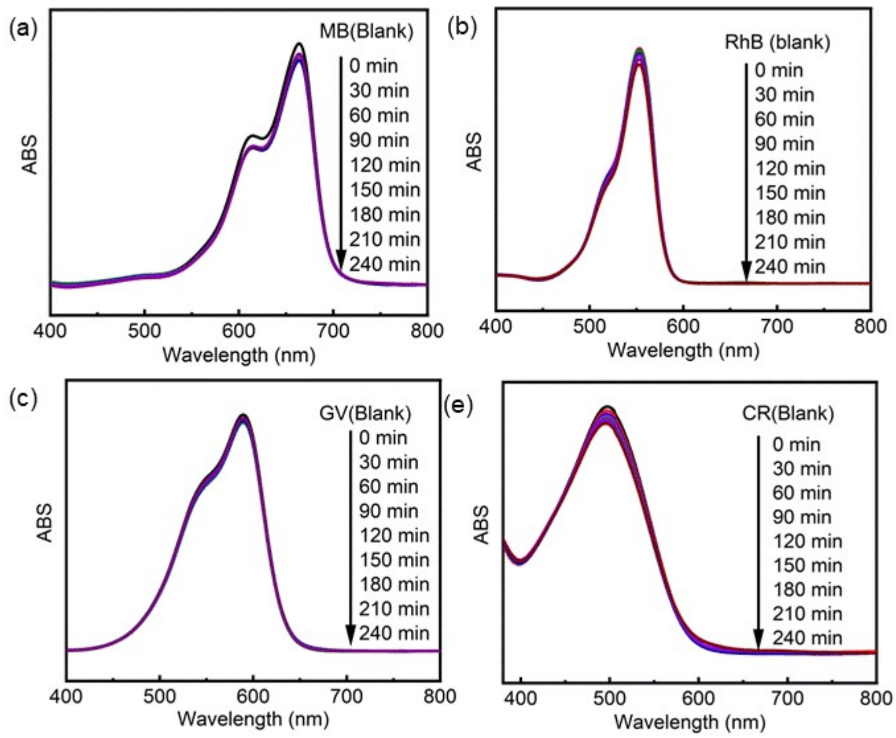

Fig. S7 UV-Vis spectra of blank experiment for dye adsorption (performed in the absence of any catalyst).

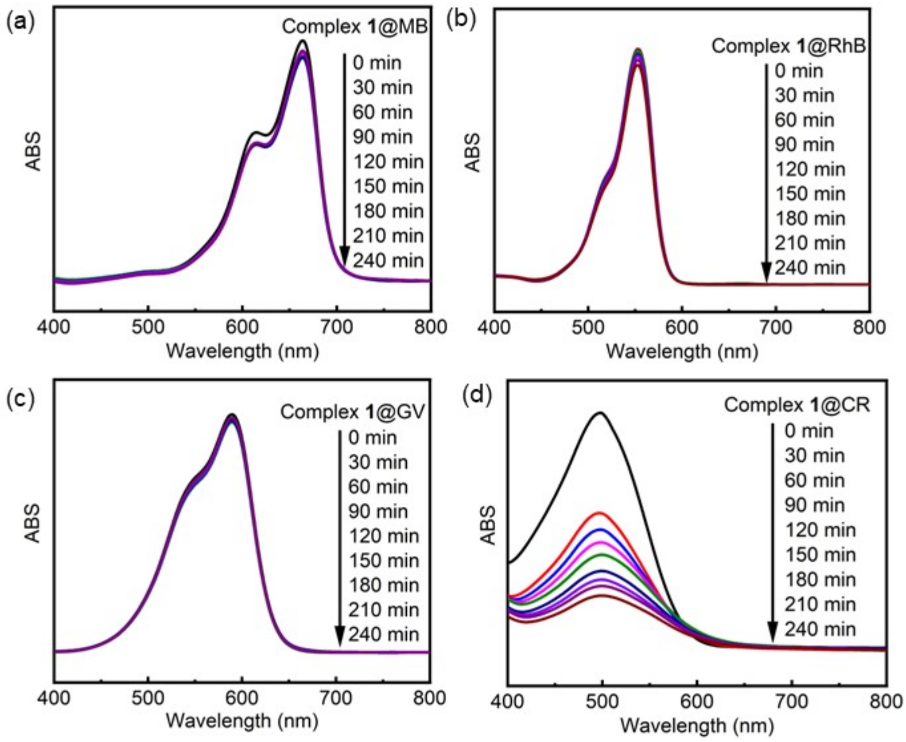

Fig. S8 UV-Vis spectra of MB (a), RhB (b), GV (c) and CR (d) solutions recorded after different adsorption times with complex **1**.

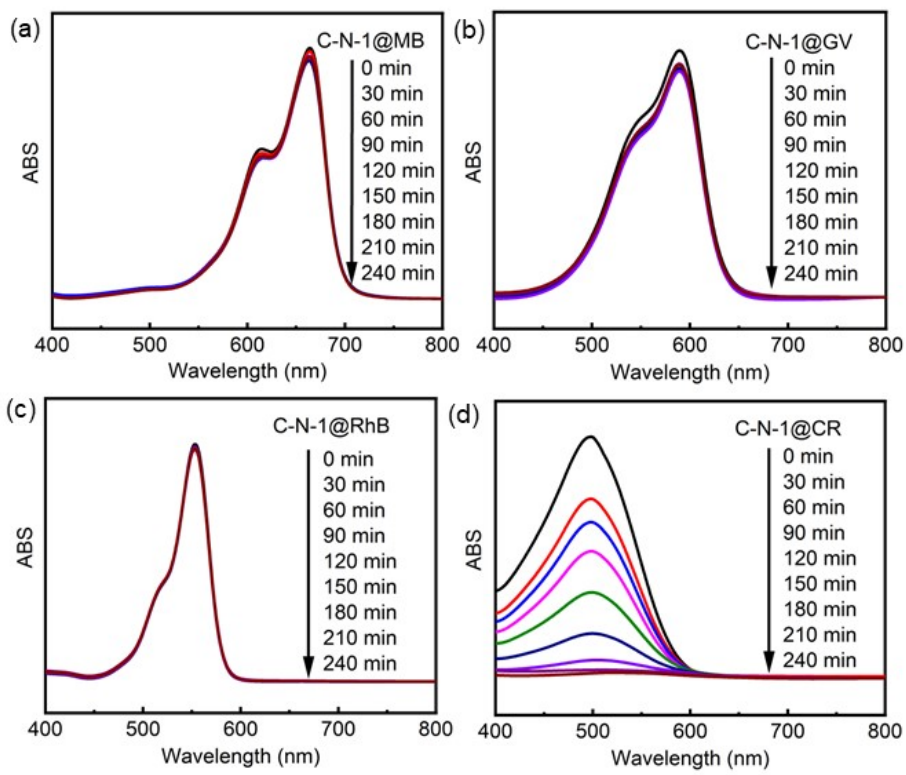

Fig. S9 UV-Vis spectra of MB (a), RhB (b), GV (c) and CR (d) solutions recorded after different adsorption times with **C-N-1**.

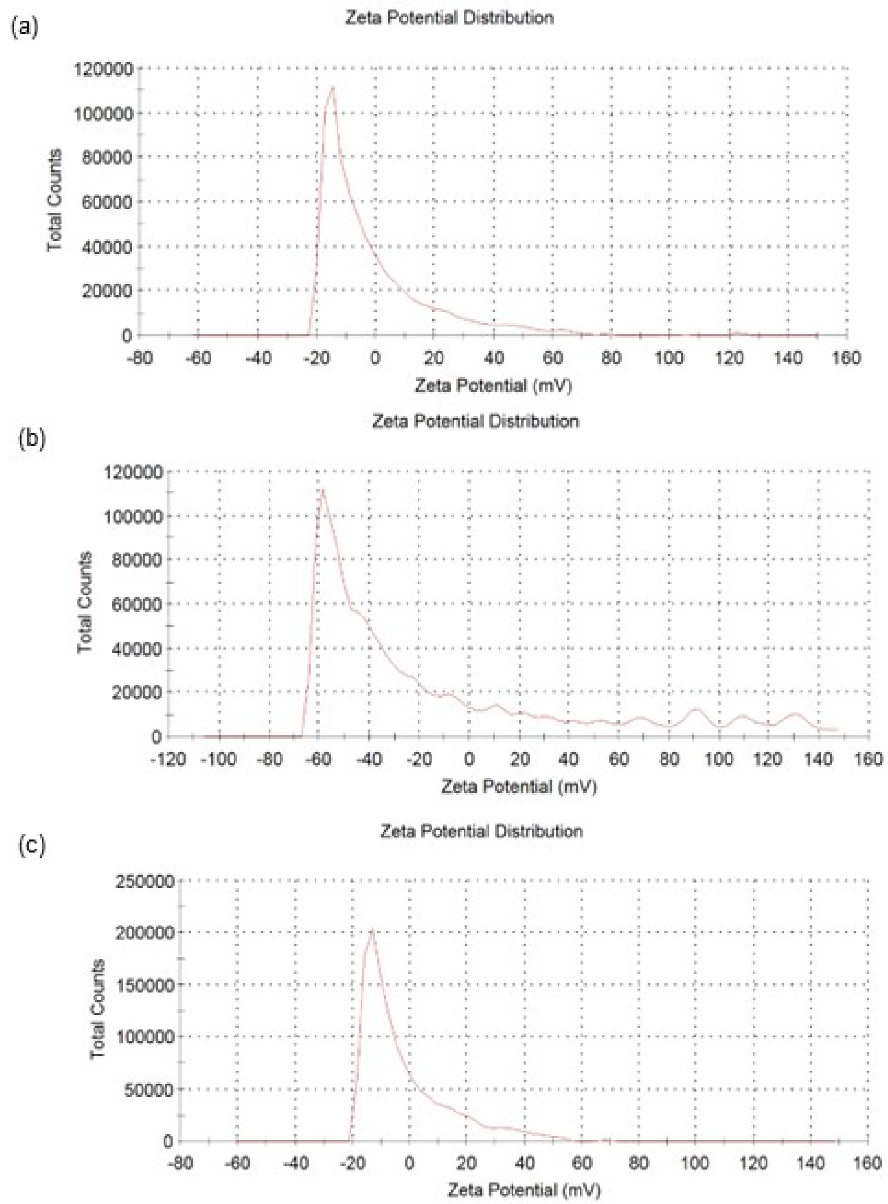

Fig. S10 The Zeta potential of complex **1** (a), **C-N-1** (b), and **C-V-1** (c).

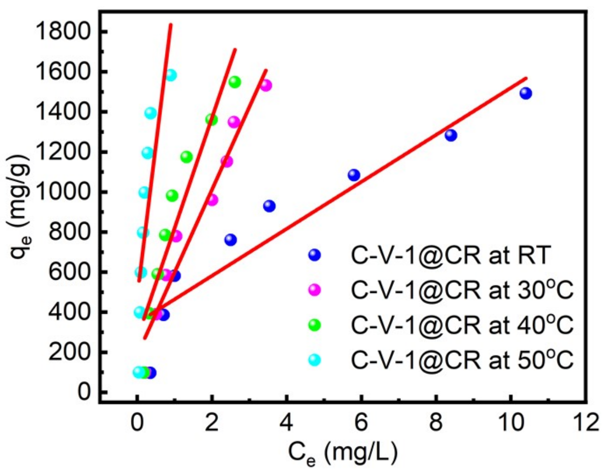

Fig. S11 Effect of different temperatures on CR adsorbed by **C-V-1**.

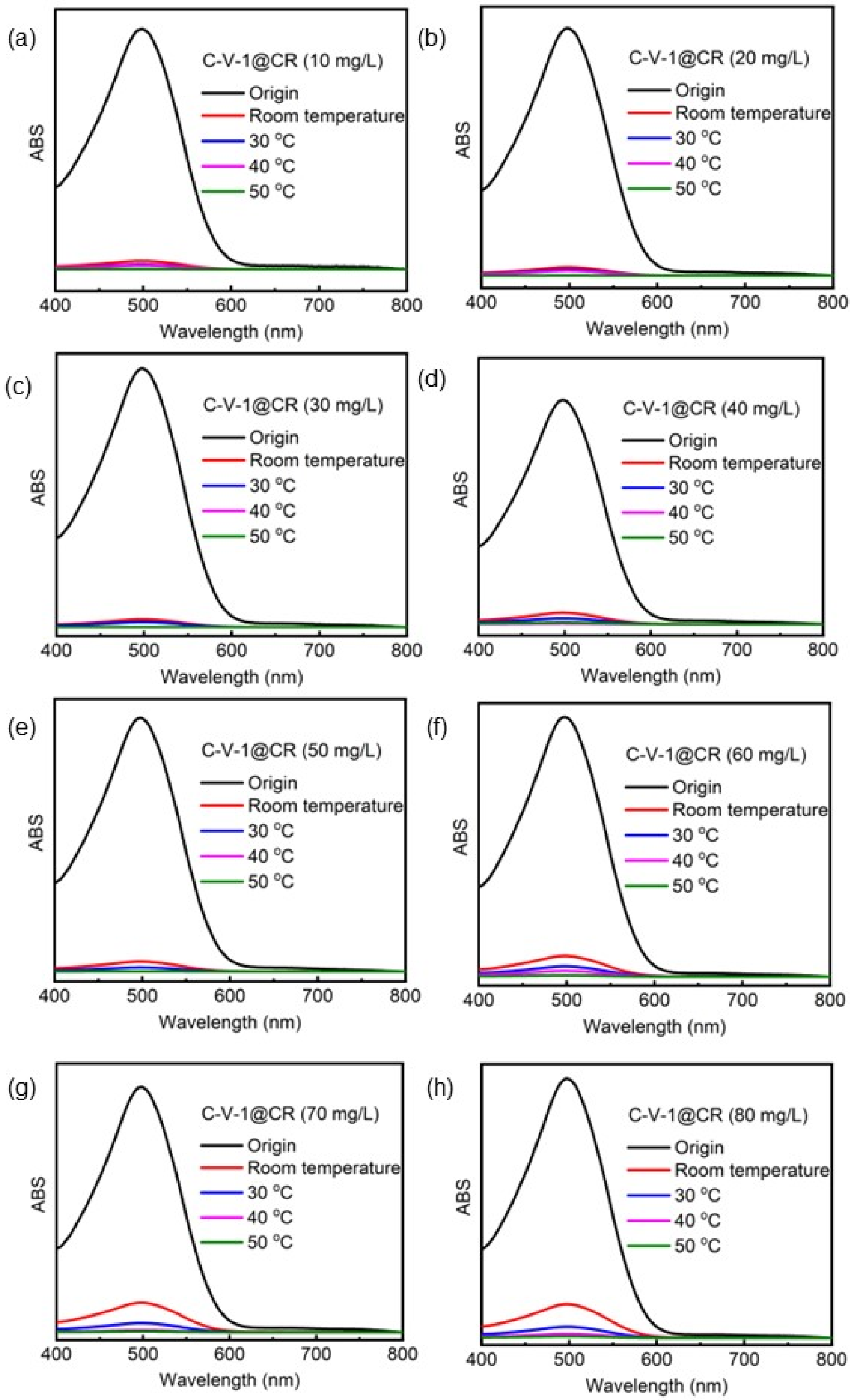

Fig. S12 UV–vis spectra of different concentrations of CR solutions after 240 min with **C-V-1** at different temperatures.

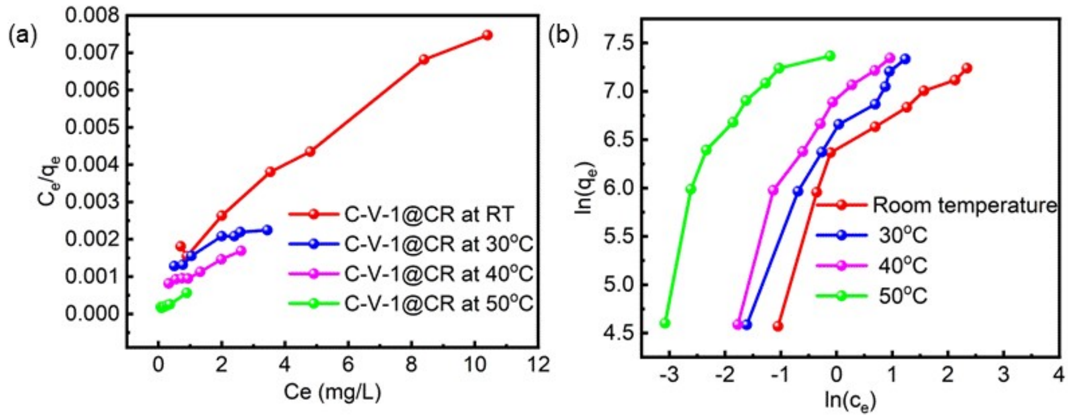

Fig. S13 (a) The equilibrium plots for the adsorption CR on to the **C-V-1** at 298, 303, 313, 323 K: Langmuir model equilibrium; (b) The equilibrium plots for the adsorption CR on to the **C-V-1** at 298, 303, 313, 323 K: Freundlich model equilibrium plots.

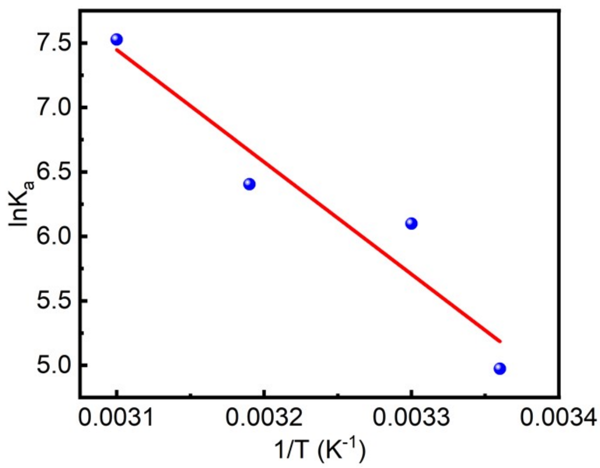

Fig. S14 The plot of $\ln K_a$–1/T for adsorption of CR on **C-V-1**.

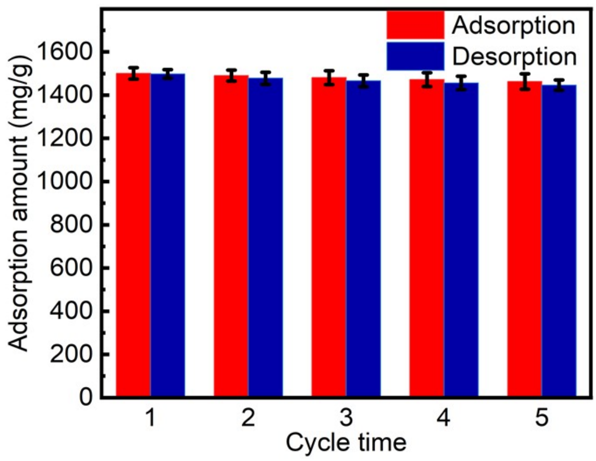

Fig. S15 The cycling stability of the adsorption/desorption of CR on **C-V-1**.

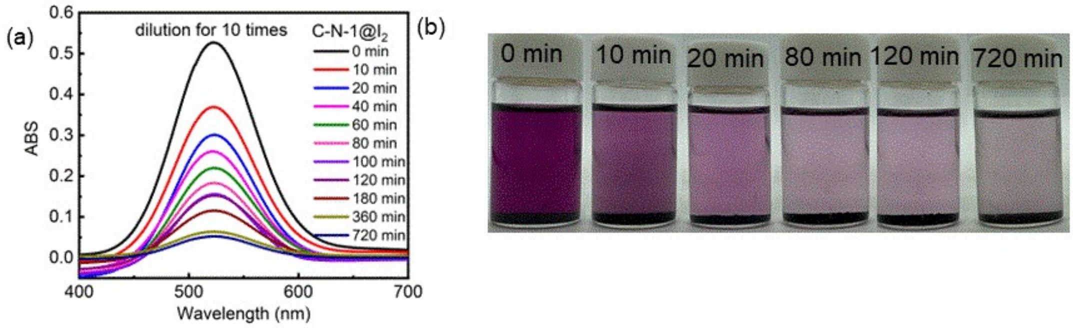

Fig. S16 (a) The UV-Vis absorption spectra of **C-N-1** for the adsorption of I_2/cyclohexane solution (5 mL, 0.005 mol L^{-1}) at 521 nm; (b) Gradual color change from dark purple to colorless by immersing **C-N-1** in I_2/cyclohexane solution (5 mL, 0.005 mol L^{-1}).

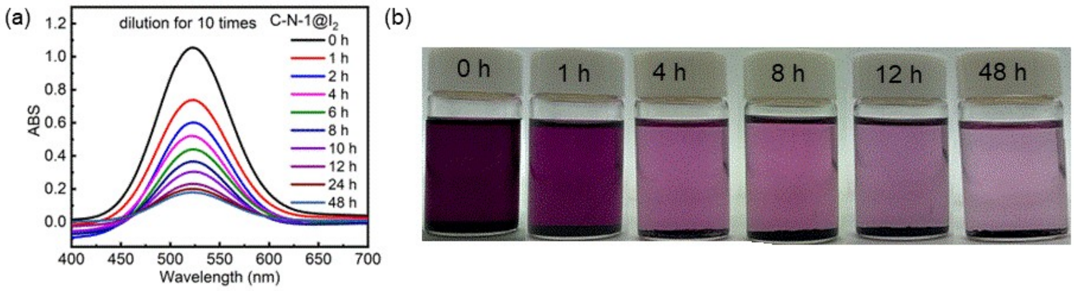

Fig. S17 (a) The UV-Vis absorption spectra of **C-N-1** for the adsorption of I_2/cyclohexane solution (5 mL, 0.01 mol L^{-1}) at 521 nm; (b) Gradual color change from dark purple to light pink by immersing **C-N-1** in I_2/cyclohexane solution (5 mL, 0.01 mol L^{-1}).

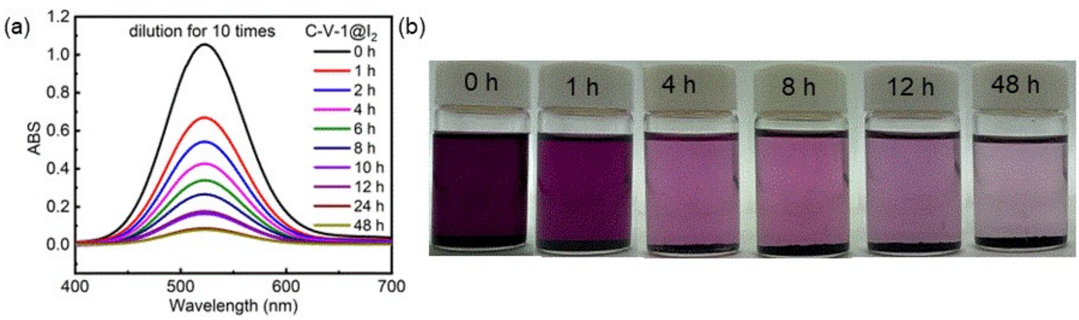

Fig. S18 (a) The UV-Vis absorption spectra of **C-V-1** for the adsorption of I_2/cyclohexane solution (5 mL, 0.01 mol L^{-1}) at 521 nm; (b) Gradual color change from dark purple to light pink by immersing **C-V-1** in I_2/cyclohexane solution (5 mL, 0.01 mol L^{-1}).

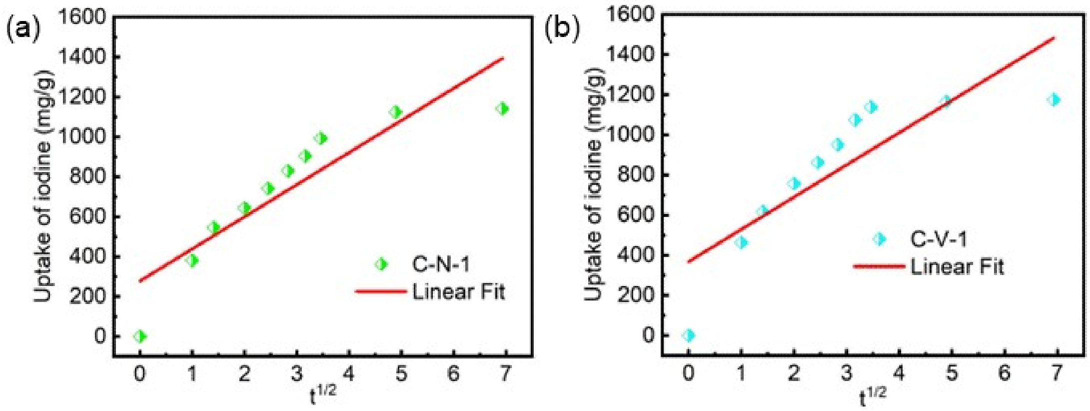

Fig. S19 The intra-particle diffusion model of iodine on **C-N-1** (a) and **C-V-1** (b).

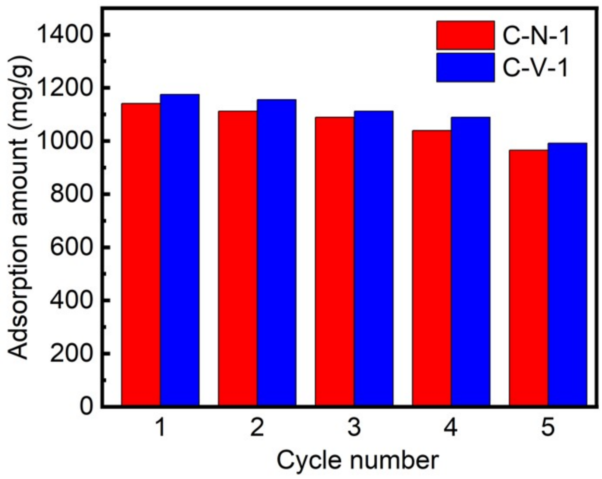

Fig. S20 (a) The iodine adsorption during four consecutive runs over adsorbent **C-V-1** and **C-N-1**.

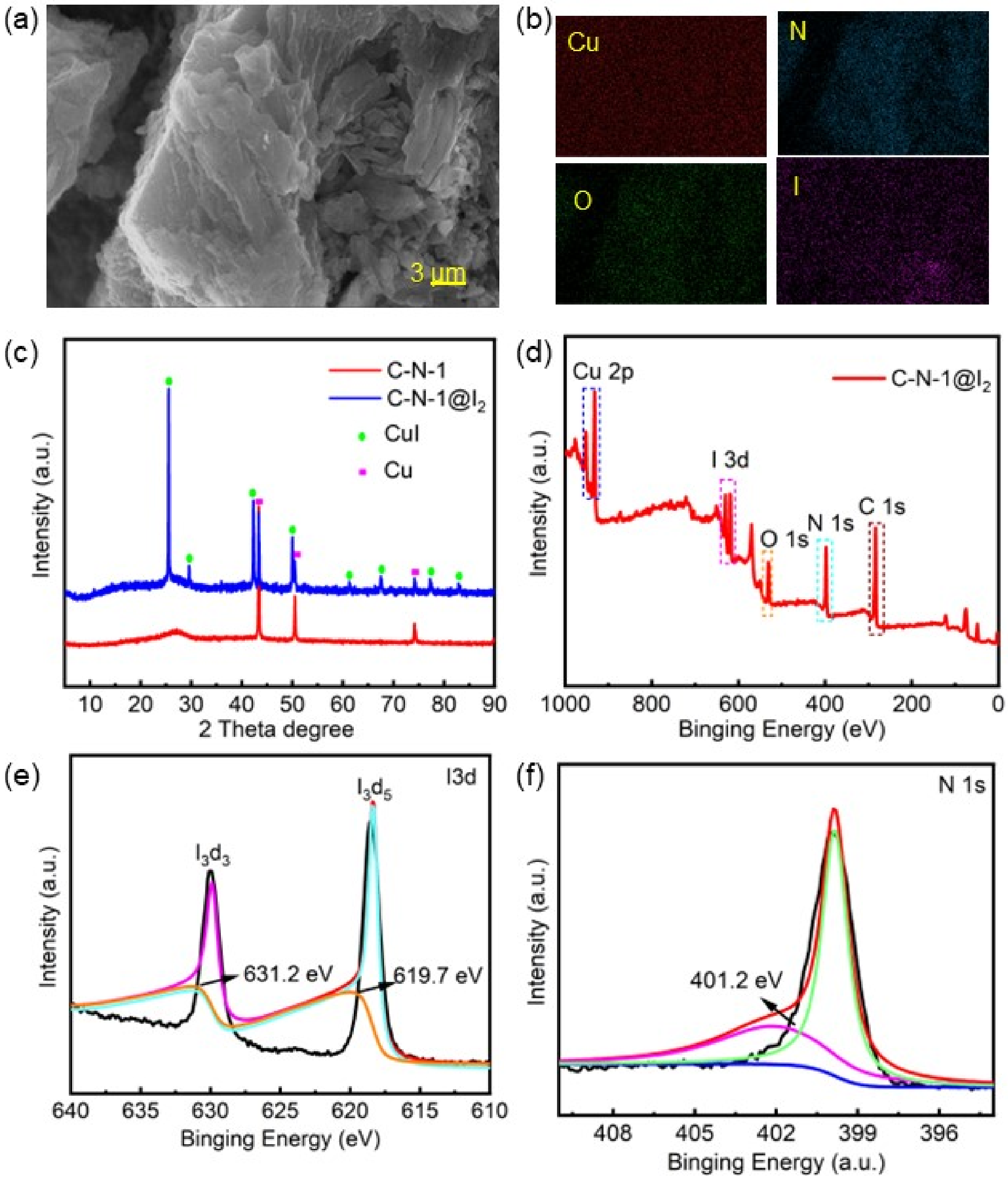

Fig. S21 (a) SEM image of **C-N-1**; (b) EDS-mapping of **C-N-1**; (c) PXRD patterns of **C-N-1** before and after Iodine adsorption; (d) XPS survey spectra after iodine for **C-N-1**; (e) XPS survey spectra of I 3d for **C-N-1**; (f) XPS survey spectra of N 1s for **C-N-1**.